Segmentation of the Geographic Atrophy in Spectral-Domain Optical Coherence Tomography and Fundus Autofluorescence Images

Zhihong Hu,[1] Gerard G. Medioni,[2] Matthias Hernandez,[2] Amirhossein Hariri,[1] Xiaodong Wu,[3] and SriniVas R. Sadda[1]

[1]Doheny Eye Institute, University of Southern California, Los Angeles, California
[2]Department of Computer Science, University of Southern California, Los Angeles, California
[3]Department of Electrical and Computer Engineering, University of Iowa, Iowa City, Iowa

Correspondence: SriniVas R. Sadda, Doheny Eye Institute, 1450 San Pablo Street, Los Angeles, CA 90033; ssadda@doheny.org.

Submitted: June 5, 2013
Accepted: November 11, 2013

Citation: Hu Z, Medioni GG, Hernandez M, Hariri A, Wu X, Sadda SR. Segmentation of the geographic atrophy in spectral-domain optical coherence tomography and fundus autofluorescence images. *Invest Ophthalmol Vis Sci*. 2013;54:8375–8383. DOI:10.1167/iovs.13-12552

Purpose. Geographic atrophy (GA) is the atrophic late-stage manifestation of age-related macular degeneration (AMD), which may result in severe vision loss and blindness. The purpose of this study was to develop a reliable, effective approach for GA segmentation in both spectral-domain optical coherence tomography (SD-OCT) and fundus autofluorescence (FAF) images using a level set–based approach and to compare the segmentation performance in the two modalities.

Methods. To identify GA regions in SD-OCT images, three retinal surfaces were first segmented in volumetric SD-OCT images using a double-surface graph search scheme. A two-dimensional (2-D) partial OCT projection image was created from the segmented choroid layer. A level set approach was applied to segment the GA in the partial OCT projection image. In addition, the algorithm was applied to FAF images for the GA segmentation. Twenty randomly chosen macular SD-OCT (Zeiss Cirrus) volumes and 20 corresponding FAF (Heidelberg Spectralis) images were obtained from 20 subjects with GA. The algorithm-defined GA region was compared with consensus manual delineation performed by certified graders.

Results. The mean Dice similarity coefficients (DSC) between the algorithm- and manually defined GA regions were 0.87 $\pm$ 0.09 in partial OCT projection images and 0.89 $\pm$ 0.07 in registered FAF images. The area correlations between them were 0.93 ($P < 0.001$) in partial OCT projection images and 0.99 ($P < 0.001$) in FAF images. The mean DSC between the algorithm-defined GA regions in the partial OCT projection and registered FAF images was 0.79 $\pm$ 0.12, and the area correlation was 0.96 ($P < 0.001$).

Conclusions. A level set approach was developed to segment GA regions in both SD-OCT and FAF images. This approach demonstrated good agreement between the algorithm- and manually defined GA regions within each single modality. The GA segmentation in FAF images performed better than in partial OCT projection images. Across the two modalities, the GA segmentation presented reasonable agreement.

Keywords: segmentation, geographic atrophy, spectral-domain optical coherence tomography images, fundus autofluorescence images

Age-related macular degeneration (AMD) is the leading cause of blindness in people over the age of 65 years in the Western world.[1] Geographic atrophy (GA), with loss of the retinal pigment epithelium (RPE) and photoreceptors, is a manifestation of the advanced or late stage of AMD, and is increasingly the main cause of vision loss in patients.[1,2] Geographic atrophy is identified clinically by the presence of depigmentation, sharply demarcated borders, and increased visibility of the underlying choroidal vessels.[1,2] Typically, the atrophic areas initially appear in the extrafoveal region in the macula,[3] with eventual growth and expansion into the fovea resulting in vision loss and ultimately legal blindness. A number of potential agents are currently under clinical investigation to determine if they are of benefit in preventing the development and growth of these atrophic lesions. Techniques to rapidly and precisely quantify atrophic lesions would appear to be of value in advancing understanding of the pathogenesis of GA lesions and the level of effectiveness of these putative therapeutics.

Historically, color fundus photography has been the gold standard method for documenting and measuring the size of GA lesions. Although GA lesions can be readily identified and demarcated in high-quality color images with good stereopsis, the borders may be more difficult to identify in monoscopic images of lower quality. More recently, fundus autofluorescence (FAF) has emerged as a useful technique to provide high contrast for the identification of GA lesions. Fundus autofluorescence imaging is a noninvasive, in vivo two-dimensional (2-D) imaging technique for metabolic mapping of naturally or pathologically occurring fluorophores of the ocular fundus.[4]

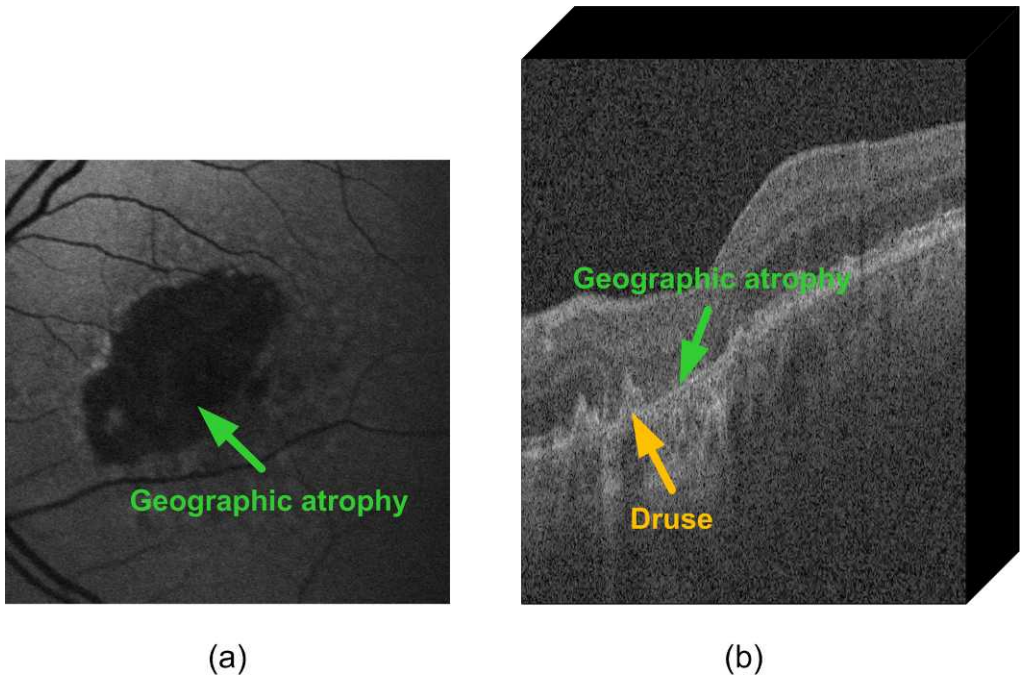

FIGURE 1. Example of geographic atrophy on a FAF image and a B-scan of a SD-OCT volume image. (**a**) The *green arrow* for the hyporeflective region in the FAF image indicates geographic atrophy. (**b**) The *green arrow* for the hyperreflective region in the B-scan of the SD-OCT image indicates geographic atrophy. The *orange arrow* indicates a druse.

When atrophy ensues, RPE cells are lost, and this concurrently results in depletion of the fluorophores (in lipofuscin) and a reduction in the autofluorescent signal (Fig. 1a). The reproducibility of measuring GA lesions by human graders using FAF imaging has been shown to be excellent, and the Food and Drug Administration (FDA) has indicated that demonstration of a reduction of GA growth may be an acceptable endpoint for registration trials. In 2011, Schmitz-Valckenberg et al.[5] reported a semiautomated image processing approach (called RegionFinder) for the identification and quantification of atrophic areas with GA on images obtained by confocal scanning laser ophthalmoscopy FAF imaging, further expanding the potential utility of this method.

Spectral-domain optical coherence tomography (SD-OCT) is an interference-based, noninvasive, in vivo imaging technique that provides a 3-D cross-sectional, microscale depiction of the optical reflectance properties of biological tissues.[6] Spectral-domain OCT can directly access the spectrum and thus provides rapid acquisition of the 3-D images of interest. Improvements to existing SD-OCT, such as frame averaging, despeckling, and enhanced image contrast, have provided even better definition of deeper intraocular structures.[7–11] For example, the outer RPE/Bruch's membrane (RPE/BM) complex and even the choroid–sclera junction can be seen in the SD-OCT images. Compared to planar imaging techniques, SD-OCT provides "true" 3-D information regarding the retina and choroid. When GA develops, loss of the RPE and the outer retinal layers can be observed on the OCT B-scans. Loss of the RPE results in increased transmission of light into deeper structures and increased reflectivity at the level of the choroid (Fig. 1b).

The purpose of this study was to develop a reliable, effective approach for GA segmentation in both SD-OCT and FAF images using a level set–based approach and to compare the segmentation performance in the two modalities.

MATERIALS AND METHODS

Subject Recruitment

Twenty subjects with late-stage AMD and evidence of GA were recruited from the University of Southern California Retina Clinics. Subjects with evidence of choroidal neovascularization (CNV; determined by imaging and ophthalmoscopic examination) were excluded, as well as patients with other ocular diseases or atrophy due to disease apart from AMD. All subjects provided written informed consent. The study was approved by the Institutional Review Board of the University of Southern California and adhered to the tenets set forth in the Declaration of Helsinki.

OCT and FAF Imaging

For each subject, both eyes underwent volume OCT imaging using Zeiss Cirrus SD-OCT (Carl Zeiss Meditec, Inc., Dublin, CA) in accordance with the existing standardized image acquisition protocol utilized by the imaging unit. All scans consisted of a macular cube scan pattern of 1024 (depth) $\times$ 512 (A-scans) $\times$ 128 (B-scans) voxels. The physical scan dimensions are $2 \times 6 \times 6$ mm. Scans were obtained with the scan oriented for vitreous zero delay. The voxel depth was 8 bits in grayscale. For each subject, one eye was randomly chosen for subsequent segmentation analysis.

The corresponding FAF images of the same subjects were obtained from a Heidelberg confocal scanning laser ophthalmoscope (cSLO) (Spectralis HRA+OCT; Heidelberg Engineering, Heidelberg, Germany), which used an optically pumped solid-state laser source to generate a blue light excitation wavelength of 488 nm for FAF images. The field of view (FOV) is $30^\circ \times 30^\circ$. The image resolution is 768×768 pixels, and the physical dimensions as provided by the camera system are 8.85 $\times$ 8.85 mm.

Investigative Ophthalmology & Visual Science

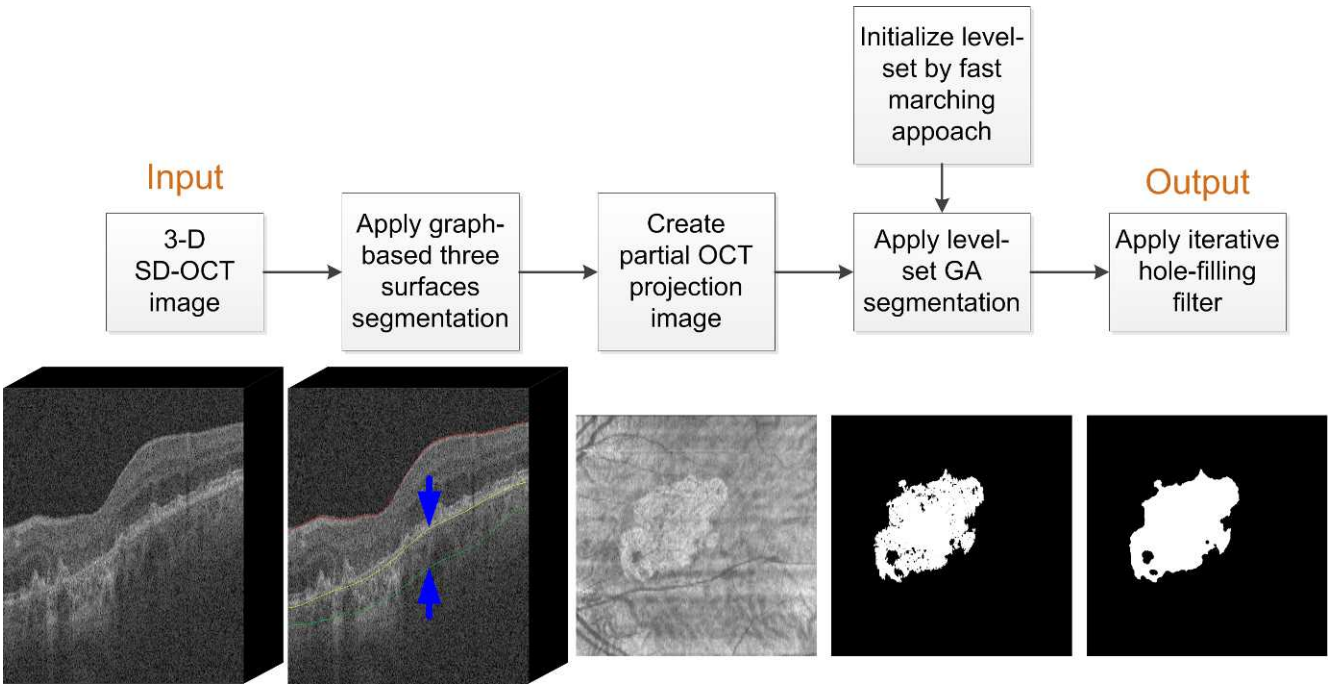

FIGURE 2. Flowchart of GA segmentation in SD-OCT images. Specifically, three retinal surfaces of ILM, RPE/BM complex, and the choroid–sclera junction were first segmented in the volumetric OCT images using a double-surface graph search scheme. A partial OCT projection image was created by averaging the intensity value between the surfaces of the RPE/BM complex and the choroid–sclera junction. A level set approach was applied to segment the GA in the partial OCT projection image with initialization by a fast marching approach. An iterative hole-filing filter was then applied to refine the GA segmentation.

Overview of the GA Segmentation

To identify the GA region in SD-OCT images, three retinal surfaces of internal limiting membrane (ILM), RPE/BM complex, and the choroid–sclera junction were first segmented in the volumetric SD-OCT images using a double-surface graph search scheme.[12] To enhance contrast for detection of the GA region in OCT volume images, we created an OCT projection image (referred to as "partial OCT projection image" against the OCT projection image created from the whole volume) based on the slab layer between the RPE/BM complex and the choroid–sclera junction, that is, the choroid. Because increased transmission of light into the choroid occurs in areas with absent or depigmented RPE, the choroid in areas of atrophy appears much brighter than adjacent areas of choroid underlying intact RPE. A level set approach was applied to segment the GA in the partial OCT projection image. Level set is a numerical method for tracking the evolution of contours and surfaces.[13,14] The central idea of the level set is to represent the evolving contour using a signed function, where its zero level corresponds to the actual contour. Level set is an implicit deformable model, also called implicit active contours, that can model arbitrarily complex shapes and topological changes. Geographic atrophy is a disease such that the progression could be of any arbitrarily irregular shape. Thus, the level set strategy is well suited for the detection of the GA region. A flowchart of GA segmentation in SD-OCT images is provided in Figure 2. In addition, the algorithm was applied in FAF images.

Construction of Partial OCT Projection Images at Choroid Layer

Prior to construction of projection images at the choroid layer, we applied our previously described graph search multilayer segmentation algorithm[12,15,16] to first simultaneously segment the ILM surface and the surface of the RPE/BM complex using a double-surface graph search scheme. A penalty to the cost function was applied at certain distances above the segmented surface of the RPE/BM complex.[12,15] The surfaces of the RPE/BM complex and the choroid–sclera junction were then simultaneously segmented using the same double-surface graph search technique.

The 2-D partial OCT projection image as described earlier was then obtained by averaging the intensity value between the surfaces of the RPE/BM complex and choroid–sclera junction in the z-direction (depth). It should be noted that the original SD-OCT volume was not isotropic (1024 [depth] $\times$ 512 [A-scans] $\times$ 128 [B-scans] voxels). To facilitate subsequent GA segmentation, an isotropic partial OCT projection image was generated by linear interpolation of the B-scans (y-direction) to enlarge the image resolution to 512 (A-scans) $\times$ 512 (B-scans) pixels. Figure 3 provides an overview of the technique, illustrating the segmentation of three surfaces and the generation of a partial OCT projection image from the choroid layer.

Geographic Atrophy Segmentation

Once the partial OCT projection images were obtained, GA segmentation was performed using a level set segmentation approach.[13,14] The underlying principle of GA detection using the level set approach is to represent the GA contour C by the zero level set of a higher-dimensional embedding function $\emptyset$, defined as the signed distance function (SDF). Inside the GA region, the function has a value of $\emptyset > 0$; outside the GA region, the function has a value of $\emptyset < 0$. Thus on the GA contour, the function has a value of $\emptyset = 0$ and hence is called the zero level set. Fundamentally, rather than directly evolving

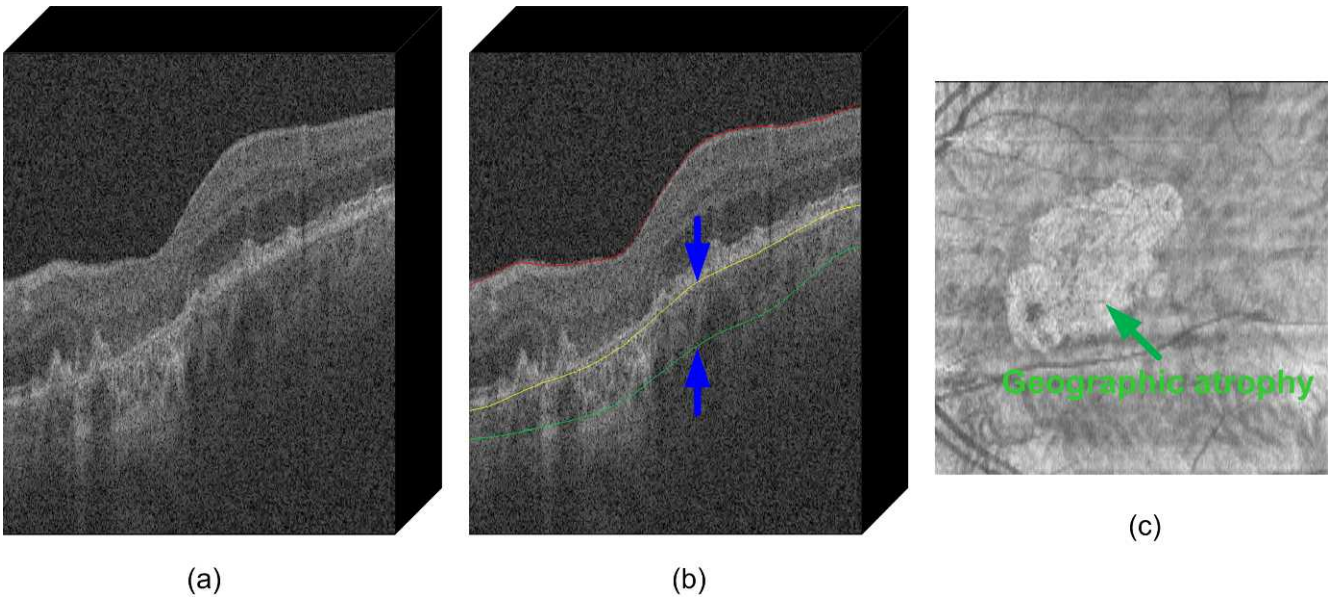

FIGURE 3. Sample illustration of three retinal layer segmentation in a SD-OCT volume and the partial OCT projection image creation. (**a**) A B-scan in a SD-OCT volume. (**b**) The B-scan overlapping with three segmented surfaces, where the *red*, *yellow*, and *green* represent the ILM, RPE/BM complex, and the choroid–sclera junction, respectively. (**c**) Partial OCT projection image created by the choroid layer indicated by the *blue arrows* in (**b**). Note that the *green arrow*–highlighted region with increased penetration indicates the GA.

the GA contour C, the algorithm evolves the level set function Ø. The level set evolution is governed by a partial differential equation (PDE) as shown in Equation 1.

$$\frac{d}{dt}\varnothing\propto - \alpha P(x,y)|\nabla\varnothing| + \beta K(x,y)|\nabla\varnothing| \qquad (1)$$

where $P(x,y)$ represents a propagation speed term; $K(x,y)$ represents a curvature term; and α and β are the weights reflecting the different influences of the propagation speed and curvature over the contour evolution. The evolving GA contour C was then obtained by extracting the zero level set.

The level set segmentation generally starts with an initial contour and gradually evolves to the zero level set representing the desired boundary/surface. Intuitively, if the initial contour is closer to the detected contour, the evolution will be faster and more efficient. The fast marching approach,[13] a simple version of the level set approach in which the level set evolution is controlled only by the propagation speed, was used to generate the initial model. More specifically, the algorithm first obtained a propagation speed image from the input partial OCT projection image by the mapping of the gradient magnitude of the partial OCT projection image, in which the high-contrast regions had low speeds and the homogeneous regions had high speed. A sigmoid function was used for the mapping of the gradient magnitude.

Seed/seeds (a seed is defined as any pixel/point inside the GA region) and an estimated GA region related to each seed were used as the initial inputs for the fast marching algorithm. Propagation then started from the seeds and traveled with the speed in the speed image. The fast marching yielded a time-crossing map, which indicated, for each pixel, the time required for the contour to reach the pixel. This outcome was then used as an initial shape model for the level set GA segmentation.

The putative GA regions in the OCT partial projection images were noted to be hyperreflective relative to adjacent nonatrophic regions. The propagation term in Equation 1 was modeled based on the intensity of the GA region as shown in Equation 2.

$$P(x,y) = \begin{cases} I(x,y) - L, & \textit{if } I(x,y) < (U-L)/2 + L \\ U - I(x,y), & \textit{otherwise} \end{cases} \qquad (2)$$

where $I(x,y)$ represents the GA image intensity at position (x,y), and U and L are the upper and lower threshold of the estimated intensity region of GA. The above equation resulted in a positive propagation term when a pixel had an intensity value within the threshold and a negative term outside the threshold. The curvature term in Equation 2 was assigned a significantly lower weight than the propagation term due to the arbitrary shape of the GA region.

Figure 4b illustrates a typical level set GA segmentation result. As a postprocessing step, a hole-filling filter was applied to fill in the holes evident in Figure 4b. The hole-filling filter iteratively converted the background pixels into the foreground when the number of foreground pixels was a majority of the neighbors until no further pixel changes occurred. Figure 4c shows the result of the hole-filling filter. The segmented 2-D GA region was then projected to the 3-D SD-OCT image, as shown in Figures 4e and 4g, to find the 3-D location.

In addition, the same level set algorithm was applied to identify the GA region in the corresponding FAF images with a specified intensity threshold region corresponding to the hypoautofluorescent property of the atrophy in FAF images. Note that the original FAF images had a broader FOV than the SD-OCT images. The FAF images were registered to the corresponding partial OCT projection images using a manual approach based on identifying multiple corresponding points between images (generally vessel crossings). The FAF images were then cropped to the same size as the partial OCT projection images. Figures 5c, 5d, and 5e illustrate the registration and the GA segmentation result in a FAF image.

Investigative Ophthalmology & Visual Science

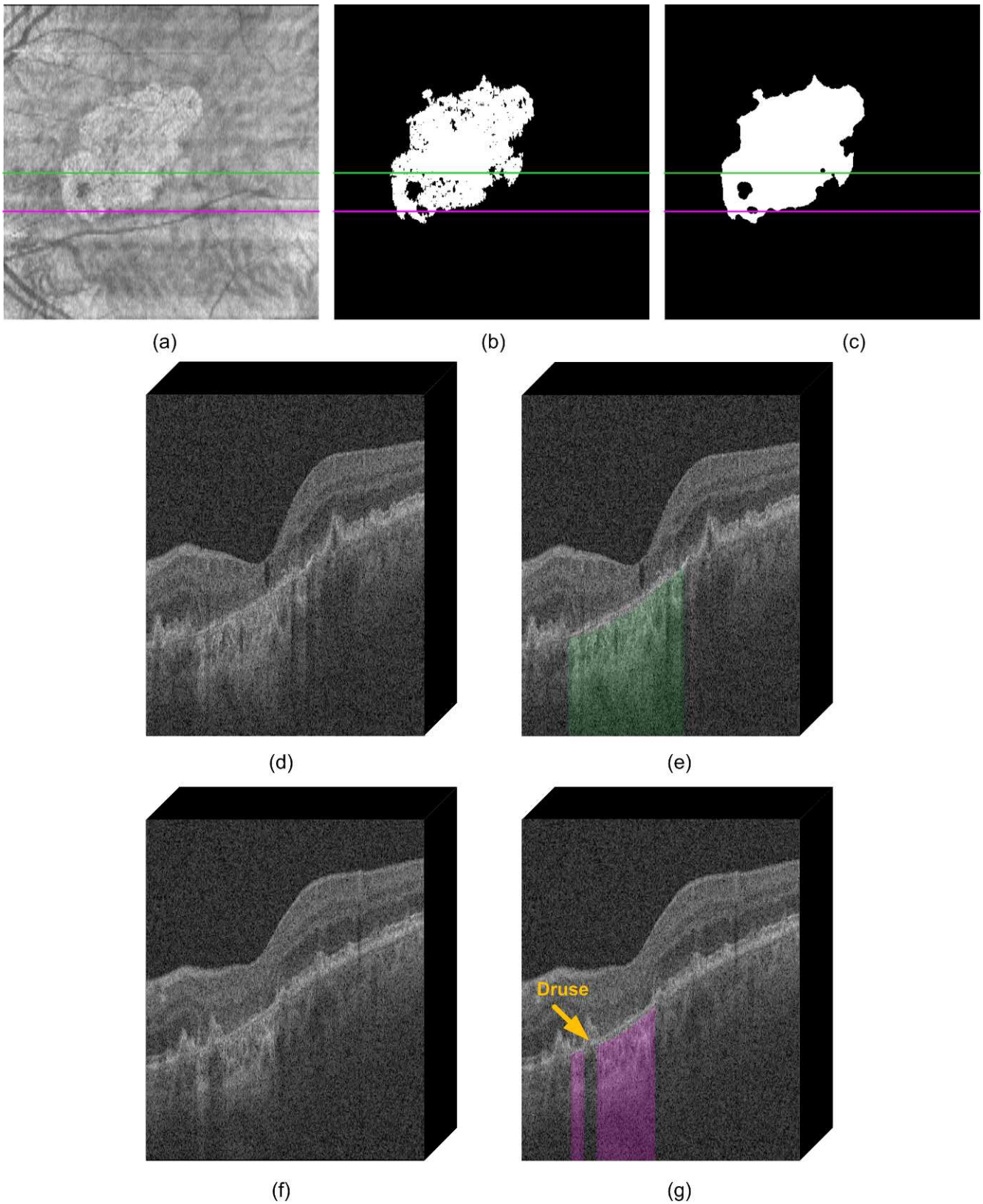

FIGURE 4. Sample illustration of GA segmentation in a SD-OCT image. (**a**) OCT partial projection image. (**b**) Level set GA segmentation result. (**c**) Geographic atrophy segmentation result after hole filling. (**d**) SD-OCT B-scan corresponding to the location indicated by the *green line* in (**a**) and (**e**) the GA segmentation (*green*) overlapping that. (**f**) SD-OCT B-scan corresponding to the location indicated by the *purple line* in (**a**) and (**b**) the GA segmentation (*purple*) overlapping that. Note that under the druse (*orange arrow*), the GA was not present.

Investigative Ophthalmology & Visual Science

Table. Comparison of Different GA Regions

	OCT Truth* vs. FAF Truth†	OCT Seg* vs. FAF Seg†	OCT Seg* vs. OCT Truth†	FAF Seg* vs. FAF Truth†	OCT Seg* vs. FAF Truth†	FAF Seg* vs. OCT Truth†
Mean DSC‡	0.89 ± 0.08	0.79 ± 0.12	0.87 ± 0.09	0.89 ± 0.07	0.83 ± 0.12	0.85 ± 0.10
r§	0.97	0.96	0.93	0.99	0.97	0.96
P value	< 0.001	< 0.001	< 0.001	< 0.001	< 0.001	< 0.001
Mean area, mm²*	6.74 ± 2.90	6.10 ± 2.74	6.10 ± 2.74	5.80 ± 2.99	6.10 ± 2.74	5.80 ± 2.99
Mean area, mm²†	6.47 ± 2.98	5.80 ± 2.99	6.74 ± 2.90	6.47 ± 2.98	6.47 ± 2.98	6.74 ± 2.90
Mean area difference, mm²	0.27 ± 0.68	0.30 ± 0.86	−0.64 ± 1.09‖	−0.67 ± 0.49‖	−0.37 ± 0.74‖	−0.94 ± 0.83‖
Absolute mean area difference, mm²	0.41 ± 0.61	0.74 ± 0.51	0.84 ± 0.93	0.68 ± 0.47	0.60 ± 0.56	0.94 ± 0.83
Mean area difference, %¶		< 0.01 ± 0.00	< 0.01 ± 0.00	< 0.01 ± 0.00	< 0.01 ± 0.00	< 0.01 ± 0.00
Absolute mean area difference, %¶		< 0.01 ± 0.00	< 0.01 ± 0.00	< 0.01 ± 0.00	< 0.01 ± 0.00	< 0.01 ± 0.00

* Mean area of the measurements in the header row.
† Mean area of the measurements in the lower row.
‡ DSC between different GA regions.
§ *r*, Pearson's correlation coefficient between different GA areas.
‖ A negative value means that the measurement in the header row is smaller than that in the lower row.
¶ Area difference in percentage was defined as the segmented GA area relative to that of the ground truth within the same image modality.

Creation of Ground Truth

To create the ground truth, a trained, certified grader (AH) from the Doheny Image Reading Center manually delineated the GA region in both the partial OCT projection images and the corresponding FAF images in an independent masked fashion. In accordance with previously published reading center protocols, the area of GA on FAF images was deemed to correspond to the zone of definite decreased autofluorescence (DDAF). DDAF is defined as one or more well-demarcated areas of decreased autofluorescence where the reduction in AF is at least 90% of the intensity level of the optic nerve or retinal vessels. This same definition has been utilized in the Age-related Eye Diseases Study 2 (AREDS2) trial. These areas of DDAF were carefully manually outlined using standard previously described planimetric grading software,[17,18] rather than detected semiautomatically with commercial region-growing techniques (e.g., Heidelberg Engineering RegionFinder), because of the desired precision in determining the exact boundary. A similar approach was used to manually delineate the atrophic lesions on the partial OCT projection images. In this case the GA lesion was defined as one or more well-demarcated areas of bright intensity compared to the background.

The reading center medical director (SRS) rereviewed and confirmed or adjusted the gradings for each case. Both graders had been shown to have excellent grading reproducibility for GA lesions in previous clinical trials. For this exercise, because we desired a high level of precision, both the initial grader and the second grader (reading center director) were asked to determine the boundary to the nearest single pixel. Thus, even a single-pixel disagreement between the initial grading and the determination of the second grader was deemed to constitute a discrepancy requiring adjustment by the second grader. The manual delineation was used as the ground truth for evaluation of the performance of the GA segmentation.

Evaluation of Segmentation Performance

To evaluate the performance of the level set GA segmentation algorithm, the algorithm-defined GA regions in the partial OCT projection images and the FAF images were compared with their ground truth, respectively. The algorithm-defined OCT GA regions were also compared against the algorithm-determined FAF GA regions. The accuracy of the level set GA segmentation was defined using the Dice similarity coefficient (DSC),[19] which measured the spatial overlap between two regions of region A and B as defined in Equation 3.

$$DSC(A,B) = 2(A \cap B)/(A+B) \quad (3)$$

In addition, Pearson's *r* was used to measure the correlation between the two regions of *A* and *B*.

Results

The Table displays the results of the quantitative comparison of the algorithm- and manually defined GA region in the partial OCT projection and registered FAF images. The mean DSC between the algorithm- and manually defined GA region in partial OCT projection images and registered FAF images are 0.87 ± 0.09 and 0.89 ± 0.07, respectively. The area correlation between the algorithm- and manually defined GA region in partial OCT projection images and FAF images are 0.93 ($P < 0.001$) and 0.99 ($P < 0.001$), respectively. The GA segmentation in FAF images is more consistent than in partial OCT projection images. The mean DSC of the algorithm-defined GA region between the partial OCT projection and registered FAF images is 0.79 ± 0.12, and the area correlation between them is 0.96 ($P < 0.001$), indicating a reasonable agreement.

The absolute mean area differences and the mean area differences in percentage within each single modality and across the multimodalities are also compared and provided in the Table. The absolute mean area differences between the algorithm- and manually defined GA region in partial OCT projection images and FAF images are –0.64 ± 1.09 and –0.67 ± 0.49 mm², respectively. The absolute mean area difference between the algorithm-defined OCT GA region and FAF GA region is 0.30 ± 0.86 mm². The mean area differences in percentage within each single modality and between the multimodalities are all less than 1%, indicating the robustness of this algorithm in both modalities.

Figures 5 and 6 illustrate the GA segmentation results in the partial OCT projection images and registered FAF images. Figure 5 is an example of a case with similar GA segmentation in the two imaging modalities, whereas Figure 6 shows a case with significant discrepancy in the GA segmentation in the two modalities.

Discussion

In this study, we described a level set approach to segment GA lesions in SD-OCT and FAF images. As shown in the Table, the algorithm- and manually defined GA regions demonstrated

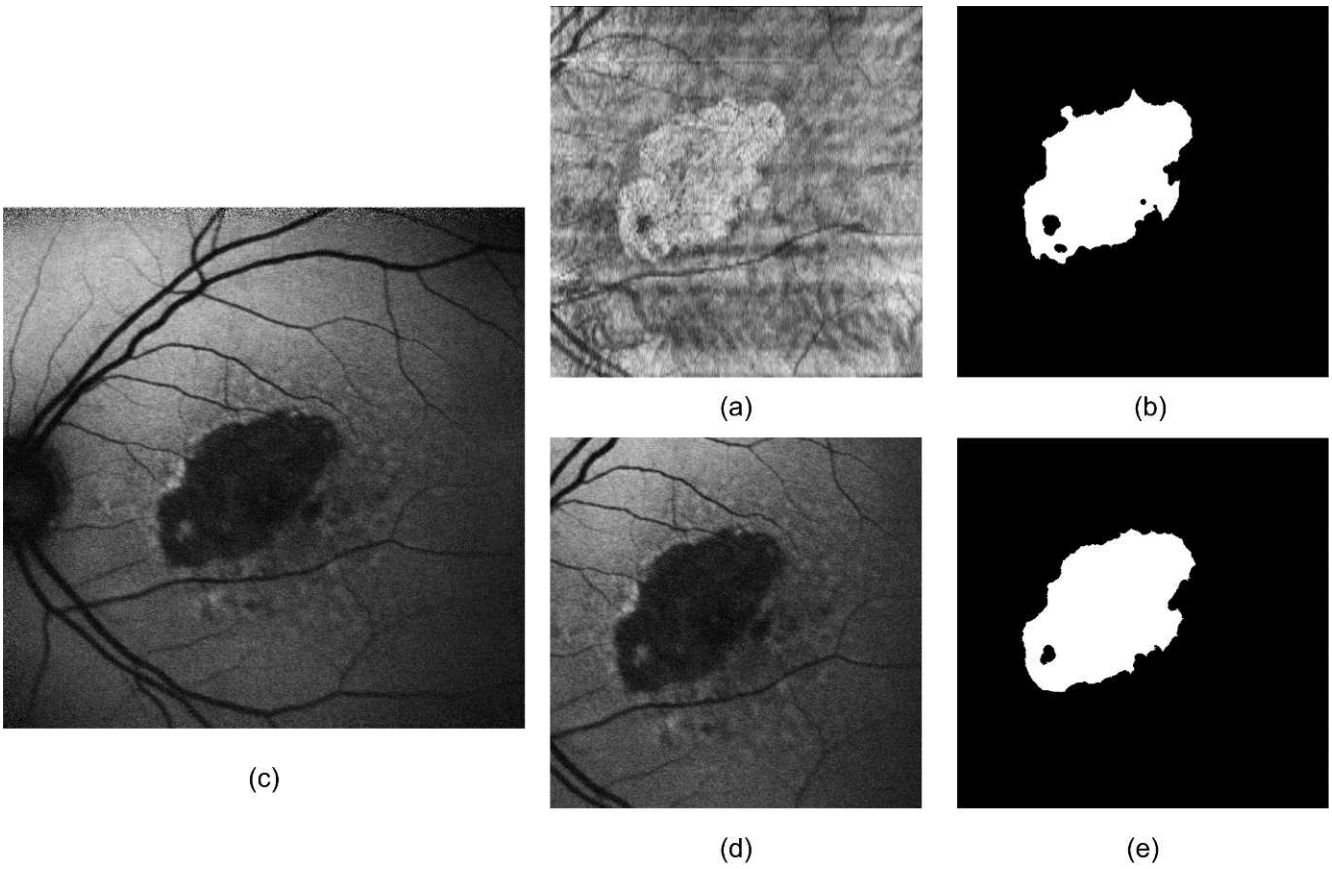

FIGURE 5. Sample illustration of GA segmentation in a partial OCT projection image and its corresponding FAF image. (**a**) Partial OCT projection image. (**b**) Geographic atrophy segmentation in the partial OCT projection image. (**c**) Original FAF image. (**d**) Registered FAF image. (**e**) Geographic atrophy segmentation in the registered FAF image. Note that the GA segmentation in OCT and FAF images performs similarly.

good agreement in both partial OCT projection (mean DSC = 0.87 ± 0.09; $r = 0.93$ [$P < 0.001$]) and FAF images (mean DSC = 0.89 ± 0.07; $r = 0.99$ [$P < 0.001$]). The GA segmentation in FAF images performed better than that in partial OCT projection images. Across the two modalities, the GA segmentation presented reasonable agreement (mean DSC = 0.79 ± 0.12; $r = 0.96$ [$P < 0.001$]).

We also compared the mean area difference and that in percentage of GA regions within each single modality and across the multimodalities. As presented in the Table, the negative mean area differences (–0.64 ± 1.09 and –0.67 ± 0.49 mm^2 in partial OCT projection and FAF images, respectively) between the segmented GA regions and their corresponding manually delineated ground truth indicate that the algorithm-defined GA in both modalities is smaller than the corresponding ground truth. The positive mean area differences (0.30 ± 0.86 mm^2) between the segmented GA regions in partial OCT projection and FAF images indicate that the algorithm-defined GA regions in partial OCT projection images are larger than in the FAF images. The mean area differences in percentage within each single modality and across the multimodalities all are less than 1%, indicating the robustness of this algorithm in both modalities.

In terms of the speed of the algorithm, the segmentation was performed on a Windows 7 workstation (Microsoft Corp., Redmond, WA) with a 2.80-GHz Intel Core i7 CPU (Intel Corp., Santa Clara, CA) of approximately 8 GB of RAM. The operating system was a 64-bit system. The mean GA segmentation time in partial OCT projection images was 23 ± 5 seconds and in FAF images was 22 ± 7 seconds, respectively. In SD-OCT volume images, to obtain the partial OCT projection images, an additional 1.7 ± 0.3 minutes was needed. Hence, the mean time for the GA segmentation in SD-OCT modality was approximately 2.1 minutes in total.

Compared to the RegionFinder approach reported by Schmitz-Valckenberg et al.,[5] which used the region-growing algorithm, the major advantage of the level set approach was that the capability of speed function could be positive in some places and negative in others, so that the front could move forward in some places and backward in others. This capability enhanced its ability to segment objects of irregular shape and recognize GA contours better than RegionFinder, which grew the region only forward. However, such theoretical advantage needs to be further validated by data, which is the goal in our next step.

Despite the favorable performance of the GA segmentation in both the SD-OCT and FAF image modalities, there are several limitations in this preliminary study. First, the SD-OCT volumetric images used in this study were anisotropic (1024 [depth] × 512 [A-scan] × 128 [B-scan] voxels). Although when creating the partial OCT projection images, we did convert to an isotropic resolution (512 [A-scan] × 512 [B-scan] pixels) by a linear interpolation between B-scans, it is possible that a more isotropic SD-OCT dataset without the need for interpolation could yield more accurate GA segmentation. Future high-speed swept-source OCT devices may be capable of yielding such datasets. Second, the OCT GA identification was based on the indirect effects of atrophy on the appearance of the choroid rather than a measurement of the atrophic lesion itself in 3-D. Thus, changes in the overlying retina such as pigment

Investigative Ophthalmology & Visual Science

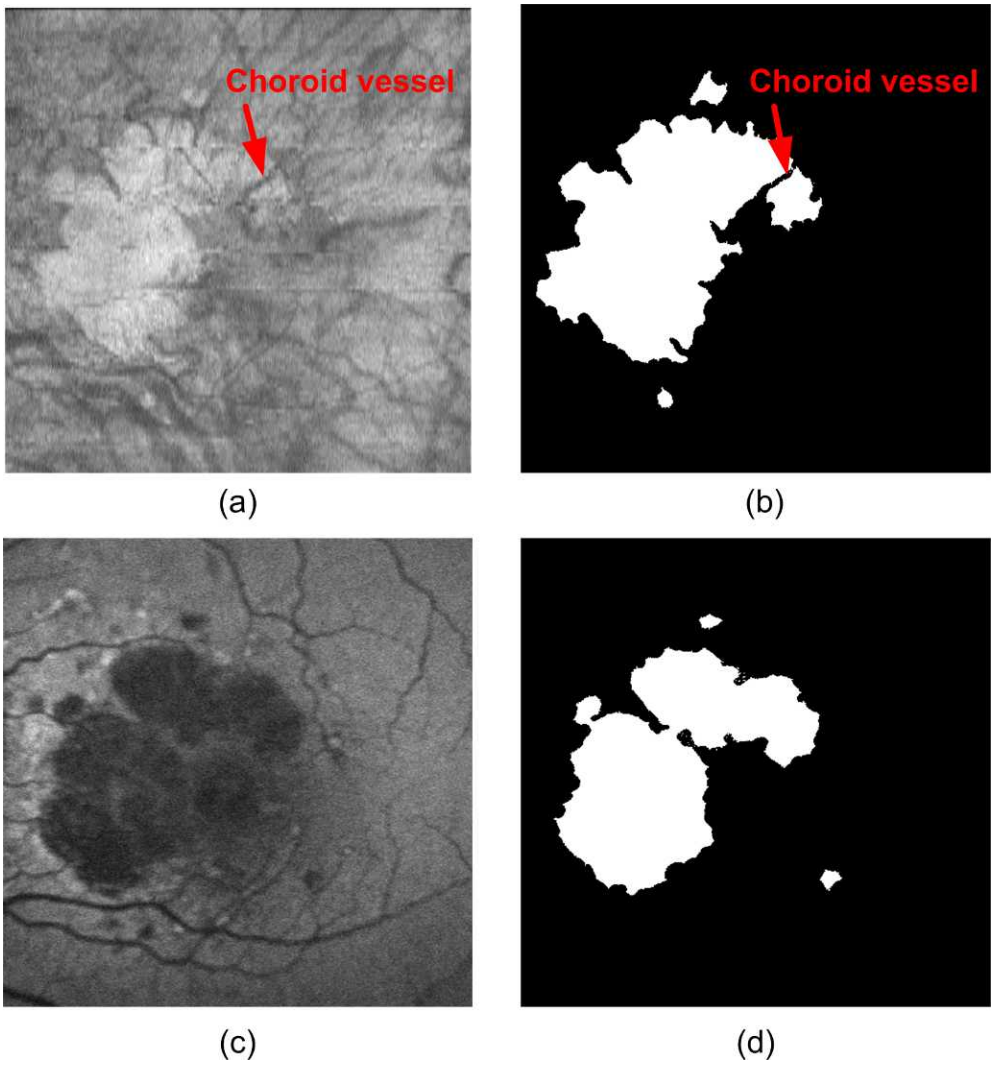

FIGURE 6. Sample illustration of GA segmentation in a partial OCT projection image and its corresponding FAF image. (**a**) Partial OCT projection image. (**b**) Geographic atrophy segmentation in the partial OCT projection image. Note the disturbance of the GA segmentation from the choroidal vessels and the oversegmentation of the GA region in the partial OCT projection image. (**c**) Registered FAF image. (**d**) Geographic atrophy segmentation in the registered FAF image.

migration with posterior shadowing could potentially confound the atrophy delineation. In the future, utilizing information from the overlying 3-D retinal layers could yield more accurate segmentation results. Another limitation is that when one is applying fast marching for the level set initialization, the seed or seeds need to be manually selected. Lastly, GA segmentation in the partial OCT projection images overall performed worse than in the FAF images. The major reason was that the image contrast of GA regions with the background in FAF images was better than that in the partial OCT projection images. In addition, since the partial OCT projection images were obtained from the choroidal layer, choroidal vessels might exist and disturb the GA segmentation. Figure 6 is an example illustrating this case. A possible solution for enhancing GA segmentation accuracy is to combine the information from both modalities, for instance, to use the FAF images to assist with better GA segmentation in OCT images.

In summary, in this study, a level set approach was developed to segment GA regions in both SD-OCT and FAF images. This approach demonstrated a good agreement between the algorithm- and manually defined GA regions within each single modality. The GA segmentation in FAF images performed better than in OCT images. Across the two modalities, the GA segmentation showed reasonable agreement.

Acknowledgments

Supported by the Beckman Macular Degeneration Research Center and a Research to Prevent Blindness Physician Scientist Award.

Disclosure: **Z. Hu**, None; **G.G. Medioni**, None; **M. Hernandez**, None; **A. Hariri**, None; **X. Wu**, None; **S.R. Sadda**, Carl Zeiss Meditec (F, C), Allergan (C), Genentech (C), Regeneron (C), Optos (F, C), Optovue, Inc. (F)

References

1. Klein R, Klein BE, Lee KE, Cruickshanks KJ, Gangnon RE. Changes in visual acuity in a population over a 15 year period: the Beaver Dam Eye Study. *Am J Ophthalmol*. 2006;142:539–549.
2. Blair CJ. Geographic atrophy of the retinal pigment epithelium: a manifestation of senile macular degeneration. *Arch Ophthalmol*. 1975;93:19–25.

Investigative Ophthalmology & Visual Science

3. Sarks JP, Sarks SH, Killingsworth MC. Evolution of geographic atrophy of the retinal pigment epithelium. *Eye*. 1988;2:552–577.
4. Schmitz-Valckenberg S, Holz FG, Bird AC, Spaide RF. Fundus autofluorescence imaging: review and perspectives. *Retina*. 2008;28:385–409.
5. Schmitz-Valckenberg S, Brinkmann CK, Alten F, et al. Semi-automated image processing method for identification and quantification of geographic atrophy in age-related macular degeneration. *Invest Ophthalmol Vis Sci*. 2011;52:7640–7646.
6. Drexler W, Fujimoto JG. State-of-the-art retinal optical coherence tomography. *Prog Retin Eye Res*. 2008;27:45–88.
7. Nielsen FD, Thrane L, Black J, Hsu K, Bjarklev A, Andersen PE. Swept-wavelength source for optical coherence tomography in the 1 μm range. *Proc SPIE*. 2005;5861:58610H.
8. Sander B, Larsen M, Thrane L, Hougaard JL, Jorgensen TM. Enhanced optical coherence tomography imaging by multiple scan averaging. *Br J Ophthalmol*. 2005;89:207–212.
9. Ferguson RD, Hammer DX, Paunescu LA, Beaton S, Schuman JS. Tracking optical coherence tomography. *Opt Lett*. 2004;29:2139–2141.
10. Spaide RF, Koizumi H, Pozzoni MC. Enhanced depth imaging spectral-domain optical coherence tomography. *Am J Ophthalmol*. 2009;148:325.
11. Malladi R, Sethian JA, Vemuri BC. Shape modeling with front propagation: a level set approach. *IEEE Trans Pattern Anal Mach Intell*. 1995;17:158–175.
12. Hu Z, Wu X, Ouyang Y, Ouyang Y, Sadda SR. Semi-automated segmentation of the choroid in spectral-domain optical coherence tomography volume scans. *Invest Ophthalmol Vis Sci*. 2013;54:1722–1729.
13. Sethian JA. *Level Set Methods and Fast Marching Methods*. Cambridge: Cambridge University Press; 1996.
14. Chen S, Radke RJ. Level set segmentation with both shape and intensity priors. *Proceedings of the IEEE International Conference on Computer Vision*. 2009:763–770.
15. Hu Z, Wu X, Hariri A, Sadda SR. Multiple layer segmentation and analysis in 3-D spectral-domain optical coherence tomography volume scans. *J Biomed Opt*. In press.
16. Hu Z, Niemeijer M, Lee K, Abràmoff MD, Sonka M, Garvin MK. Automated segmentation of the optic disc margin in 3-D optical coherence tomography images using a graph-theoretic approach. *Proc SPIE Medical Imaging*. 2009;7262:72620U.
17. Sadda SR, Liakopoulos S, Keane PA, et al. Relationship between angiographic and optical coherence tomographic (OCT) parameters for quantifying choroidal neovascular lesions. *Graefes Arch Clin Exp Ophthalmol*. 2010;248:175–184.
18. Liakopoulos S, Ongchin S, Bansal A, et al. Quantitative optical coherence tomography findings in various subtypes of neovascular age-related macular degeneration. *Invest Ophthalmol Vis Sci*. 2008;49:5048–5054.
19. Kaus MR, Haker SJ, Wells WM III, Jolesz FA, Kikinis R. Statistical validation of image segmentation quality based on a spatial overlap index. *Acad Radiol*. 2004;11:178–189.

Investigative Ophthalmology & Visual Science